Using multifiber beams to account for shear and torsion. Applications to concrete structural elements

Jacky Mazars, Panagiotis Kotronis, Frédéric Ragueneau, Géraldine Casaux

Using multifiber beams to account for shear and torsion Applications to concrete structural elements

J. Mazars [a], P. Kotronis [a,*], F. Ragueneau [b], G. Casaux [b]

[a] *Laboratoire Sols, Solides, Structures (3S), Domaine Universitaire, BP 53, 38041 Grenoble Cedex 9, France*
[b] *Laboratoire de Me´canique et Technologie, 94235 Cachan Cedex, France*

The purpose of this work is to investigate solutions for an enhanced multifiber beam element accounting for shear and torsion. Higher order interpolations functions are used to avoid any shear locking phenomena and the cross section warping kinematics is extended to non-linear behavior using advanced constitutive laws. The efficiency of the proposed modeling strategies is tested with experimental results of concrete structural elements subjected to severe loading.

Keywords: Multifiber beams; Concrete

1. Introduction

In order to design and study the behavior of reinforced concrete (R/C) buildings in high seismicity areas, one usually follows the capacity design procedure [1–3] and uses tools such as modal analysis or push-over analysis [4–6]. An alternative choice is to perform non-linear time history calculations assuming an accurate description of materials, a 2D or 3D spatial discretization and to apply transient loadings on the structure (natural or artificial ground motions, [4]). This is currently the most refined tool of analysis for predicting the ultimate behavior of concrete structures.

However, due to excessive computational costs this approach is not commonly used in Earthquake Engineering. Non-linear dynamic analysis of complex civil engineering structures based on a detailed finite element model requires large-scale computations and involves delicate solution techniques. The necessity to perform parametric studies due to the stochastic characteristic of the input accelerations imposes simplified numerical modeling that reduces the computational cost. In this work, the latter is achieved by adopting a multifiber beam model for representing the global behavior of the structural components of a complex civil engineering structure. The constitutive laws remain however sufficiently general to take into account all the different inelastic phenomena (cracking by damage, permanent deformation by plasticity and crack-closing by unilateral contact condition).

The classical approach when using multifiber beam elements is to neglect shear effects and to consider that sections remain plane and perpendicular to the neutral axis of the beam (Euler–Bernoulli hypothesis). The purpose of this article is to study solutions for a multifiber beam element capable of reproducing shear (sections remain plane but not necessarily perpendicular to the neutral axis—Timoshenko theory) or shear due to torsion. For the first case the possibility of using higher order interpolation functions to avoid any shear locking phenomena is investigated. For the second case, in order to

* Corresponding author. Tel.: +33 4 76 82 51 75; fax: +33 4 76 82 70 00.
E-mail address: Panagiotis.kotronis@inpg.fr (P. Kotronis).

account for non-linear torsion the cross section warping kinematics is studied in the framework of elasticity and extended to non-linear behavior using advanced constitutive laws. The effects of warping on the damage kinematics and the crack pattern of the cross section are studied and their influences on the global behavior of structural members are analyzed.

The efficiency of the proposed modeling strategies is validated with experimental results on three concrete elements submitted to severe loading. A cantilever-type R/C column specimen, a U-shaped R/C wall and a plain concrete beam subject to pure torsion. Comparisons between experiments and computations give an insight into the approach.

2. Constitutive laws

Both steel and concrete are described within the thermodynamic framework for irreversible processes [7]. In order to reproduce correctly the behavior of reinforcement bars, we choose a classical plasticity model accounting for the non-linear kinematic hardening of Armstrong and Frederick [8]. A typical stress–strain response curve predicted by this model is given in Fig. 1.

Constitutive laws for concrete are based on the principles of damage mechanics following the usual approach [7]: After choosing the state variables and the expression of free energy, derivations give the state laws that lead to the constitutive equations. Two different models are presented hereafter, the first adapted to monotonic loadings having one scalar damage variable, and the second adapted to cyclic loadings having two scalar damage variables and including crack closure and permanents effects.

2.1. Mazars damage model for concrete [9]

Concrete—like most of the geomaterials and ceramics—is perceived like brittle in tension and more ductile under compression loading. During experimental tests, a network of microscopic cracks nucleates perpendicularly to the direction of extension, which coalesce until complete rupture. Whereas under uniaxial tension a single crack propagates, under compression and due to the presence of heterogeneities in materials (aggregate surrounded by a cement matrix) tensile transverse strains generate a self-equilibrated stress field orthogonal to the loading direction. A pure mode I (extension) is thus considered to describe the behavior in compression.

The influence of microcracking due to external loads is introduced via a single scalar damage variable D ranging from 0 (undamaged material) to 1 (completely damaged material). The free energy ψ for this model takes the following form:

$$\rho\psi = \frac{1}{2}\boldsymbol{\varepsilon} : H(D) : \boldsymbol{\varepsilon}, \tag{1}$$

$H(D)$ is the Hooke elasticity tensor depending on the actual value of D through the form $H(D) = H_0(1 - D)$, H_0 being the elasticity tensor for the virgin material. From the state equations, $\boldsymbol{\sigma} = \rho\partial\psi/\partial\boldsymbol{\varepsilon}$, the constitutive state law for a scalar damage model coupled to elasticity leads to

$$\boldsymbol{\sigma} = (1 - D)\left[K\,\mathrm{Tr}(\boldsymbol{\varepsilon})\mathbf{I} + 2G\left(\boldsymbol{\varepsilon} - \frac{1}{3}\mathrm{Tr}(\boldsymbol{\varepsilon})\mathbf{I}\right)\right] \tag{2}$$

or

$$\boldsymbol{\varepsilon} = 1/E(1 - D)[(1 + v)\boldsymbol{\sigma} - v\,\mathrm{Tr}(\boldsymbol{\sigma})\mathbf{I}], \tag{3}$$

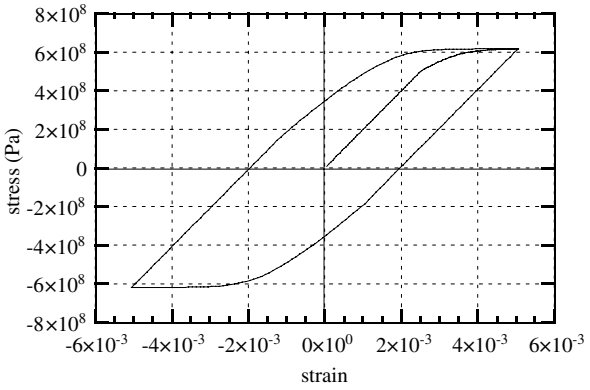

Fig. 1. Cyclic behavior for the steel model.

K and G are the bulk modulus and the shear modulus respectively, E and ν the Young's modulus and the Poisson's ration. $\mathbf{I}$ denotes the identity tensor. In order to introduce the non-symmetric behavior of concrete, the failure criterion is expressed in terms of the principal extensions. An equivalent strain is defined as

$$\varepsilon_{\text{eq}} = \sqrt{\sum_{i=1}^{3} \langle \varepsilon_i \rangle_+^2}, \tag{4}$$

where $\langle \bullet \rangle_+$ is the Macauley bracket and ε_i are the principal strains. The yield criterion of damage follows accounting for isotropic hardening $\kappa(D)$:

$$f(\varepsilon, d) = \varepsilon_{\text{eq}} - \kappa(D). \tag{5}$$

Two evolution laws for damage are considered for tension and compression (index i refers either to traction or compression):

$$D_i = 1 - \frac{\varepsilon_{\text{d0}}(1 - A_i)}{\varepsilon_{\text{eq}}} - A_i \exp(-B_i(\varepsilon_{\text{eq}} - \varepsilon_{\text{d0}})), \tag{6}$$

ε_{d0} is the initial damage threshold; A_i and B_i are material parameters. The resulting damage to be introduced in the constitutive equation is a combination of those two scalar damage variables using the following weighting coefficients α_t and α_c [9]:

$$D = \alpha_t^{\beta} D_t + \alpha_c^{\beta} D_c. \tag{7}$$

We call σ_+ and σ_- ($\sigma = \sigma_+ + \sigma_-$) the tensors in which appear only the positive and negative principal stress, respectively, and ε_t, ε_c the strain tensors defined as

$$\varepsilon_t = \Lambda^{-1} : \sigma_+ \quad \text{and} \quad \varepsilon_c = \Lambda^{-1} : \sigma_-, \tag{8}$$

$\Lambda(d)$ is a fourth-order symmetric tensor interpreted as the secant stiffness matrix and it is a function of damage. The weights α_t and α_c are defined by the following expressions:

$$\alpha_t = \sum_{1}^{3} H_i \frac{\varepsilon_{ti}(\varepsilon_{ti} + \varepsilon_{ci})}{\varepsilon_{\text{eq}}^2}, \quad \alpha_c = \sum_{1}^{3} H_i \frac{\varepsilon_{ci}(\varepsilon_{ti} + \varepsilon_{ci})}{\varepsilon_{\text{eq}}^2}, \tag{9}$$

α_t and α_c define the contribution of each type of damage. α_t (respectively α_c) ranges from 0 (pure 3D compression state—respectively traction state) to 1 (pure 3D traction state—respectively compression state). $H_i = 1$ if $\varepsilon_i = \varepsilon_{ci} + \varepsilon_{ti} \geqslant 0$, otherwise $H_i = 0$. From Eq. (9) it can be verified that for uniaxial tension $\alpha_t = 1$, $\alpha_c = 0$, $D = D_t$ and vice versa for compression. β is a shear factor, generally equal to 1.06. Responses under compression and tension of this model are presented in Fig. 2.

2.2. La Borderie damage model for concrete [10]

A model suitable for cyclic loading has to take into account some observed phenomena such as decrease in material stiffness due to cracking, stiffness recovery which occurs at crack closure and inelastic strains concomitant to damage.

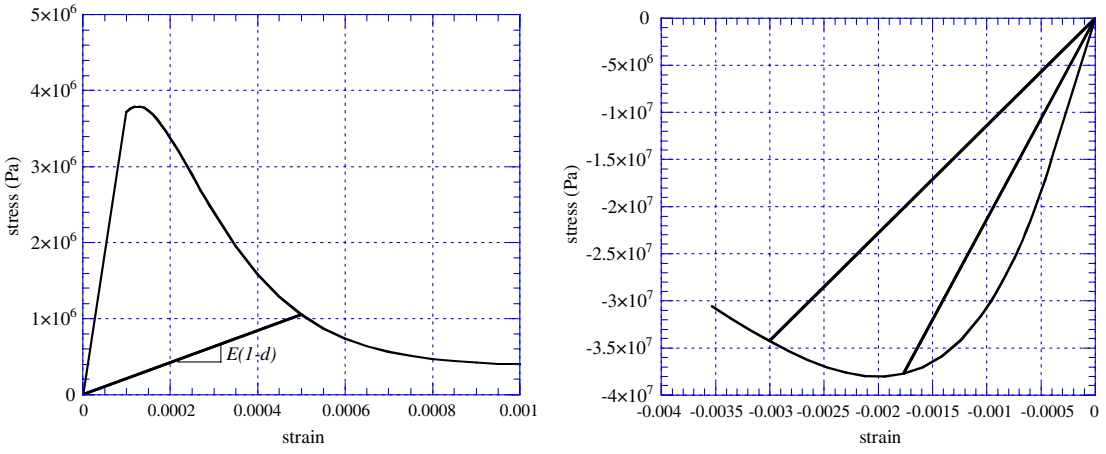

Fig. 2. Response of the Mazars damage model for concrete in tension and compression.

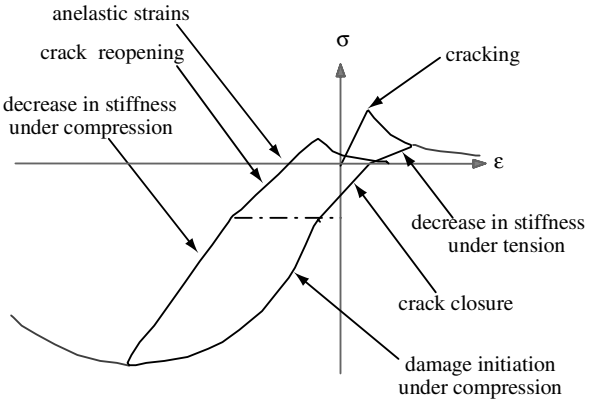

Fig. 3. Uniaxial response of the La Borderie damage model for concrete under cyclic loading.

Due to the crack closure effect, damage is deactivated and inelastic strains in the direction of extension disappear when passing from the tension to compression. To simulate this behavior two different scalar variables are used, D_1 for damage in tension and D_2 for damage in compression [10]. Inelastic strains are taken into account thanks to an isotropic tensor. The Gibbs free energy of this model in its 3D formulation can be expressed as

$$\chi = \frac{\langle \boldsymbol{\sigma} \rangle_+ : \langle \boldsymbol{\sigma} \rangle_+}{2E(1-D_1)} + \frac{\langle \boldsymbol{\sigma} \rangle_- : \langle \boldsymbol{\sigma} \rangle_-}{2E(1-D_2)} + \frac{v}{E}\left(\boldsymbol{\sigma} : \boldsymbol{\sigma} - \mathrm{Tr}(\boldsymbol{\sigma}^2)\right) + \frac{\beta_1 D_1}{E(1-D_1)} f(\boldsymbol{\sigma}) + \frac{\beta_2 D_2}{E(1-D_2)} \mathrm{Tr}(\boldsymbol{\sigma}), \tag{10}$$

$f(\boldsymbol{\sigma})$ is the crack closure function. $\langle . \rangle_+$ denotes the positive part of a tensor. E is the initial Young's modulus and v the Poisson ratio. β_1 and β_2 are material constants. From this, the state laws lead to the expression of the total strain:

$$\boldsymbol{\varepsilon} = \boldsymbol{\varepsilon}^{\mathrm{e}} + \boldsymbol{\varepsilon}^{\mathrm{in}}, \tag{11}$$

$$\boldsymbol{\varepsilon}^{\mathrm{e}} = \frac{\langle \boldsymbol{\sigma} \rangle_+}{E(1-D_1)} + \frac{\langle \boldsymbol{\sigma} \rangle_-}{E(1-D_2)} + \frac{v}{E}(\boldsymbol{\sigma} - \mathrm{Tr}(\boldsymbol{\sigma})\mathbf{I}), \tag{12}$$

$$\boldsymbol{\varepsilon}^{\mathrm{in}} = \frac{\beta_1 D_1}{E(1-D_1)} \frac{\partial f(\boldsymbol{\sigma})}{\partial \boldsymbol{\sigma}} + \frac{\beta_2 D_2}{E(1-D_2)} \mathbf{I}, \tag{13}$$

with $\boldsymbol{\varepsilon}^{\mathrm{e}}$ the elastic strains and $\boldsymbol{\varepsilon}^{\mathrm{in}}$ the inelastic strains. One can notice that if $D_1 = D_2 = D$, Eq. (12) is the same as Eq. (3) and if $\boldsymbol{\varepsilon}^{\mathrm{in}}$ is not considered ($\beta_1 = \beta_2 = 0$) the two models are the same.

Damage criteria are expressed as $f_i = Y_i - Z_i$ ($i = 1$ for tension or 2 for compression, Y_i is the associated force to the damage variable D_i and Z_i a threshold dependent on the hardening variables). The evolution laws for the damage variables D_i are written as

$$D_i = 1 - \frac{1}{1 + [A_i(Y_i - Y_{0i})]^{B_i}}, \tag{14}$$

Y_{0i} = initial elastic threshold ($Y_{0i} = Z_i(D_i = 0)$), A_i, B_i material constants. $\partial f(\sigma)/\partial\sigma$ controls the crack-closure effects depending on the actual stress state as follows:

$$\begin{cases} \mathrm{Tr}(\boldsymbol{\sigma}) \in [0, +\infty) \rightarrow \dfrac{\partial f(\boldsymbol{\sigma})}{\partial \boldsymbol{\sigma}} = \mathbf{I}, \\ \mathrm{Tr}(\boldsymbol{\sigma}) \in [-\sigma_{\mathrm{f}}, 0) \rightarrow \dfrac{\partial f(\boldsymbol{\sigma})}{\partial \boldsymbol{\sigma}} = \left(1 - \dfrac{\mathrm{Tr}(\boldsymbol{\sigma})}{\sigma_{\mathrm{f}}}\right)\mathbf{I}, \\ \mathrm{Tr}(\boldsymbol{\sigma}) \in (-\infty, -\sigma_{\mathrm{f}}) \rightarrow \dfrac{\partial f(\boldsymbol{\sigma})}{\partial \boldsymbol{\sigma}} = 0 \cdot \mathbf{I}, \end{cases} \tag{15}$$

σ_{f} being the crack closure stress.

Fig. 3 gives a schematic stress–strain response of that model for a uniaxial traction–compression loading path.

3. Multifiber beam accounting for shear

In order to simulate—in a simplified manner—the 3D behavior of concrete elements under cyclic or dynamic loading, a 3D multifiber Timoshenko beam element has been developed [11–13]. The element is displacement-based (see also [14] or [15] for an element with a forced based formulation) and can be implemented to any general-purpose finite element code without major modifications. The user defines at each fiber a material and the appropriate constitutive law. The element

takes into account deformations due to shear and has higher order interpolation functions to avoid any shear locking phenomena (cubic and quadratic Lagrangian polynomials are used for the transverse and rotational displacements respectively). The interpolation functions take the following form [16]:

$$\{U_s\} = [N]\{U\}, \tag{16}$$

$$\{U_s\}^T = \{\, u_s(x) \quad v_s(x) \quad w_s(x) \quad \theta_{sx}(x) \quad \theta_{sy}(x) \quad \theta_{sz}(x) \,\}, \tag{17}$$

$$\{U\}^T = \{\, u_1 \quad v_1 \quad w_1 \quad \theta_{x1} \quad \theta_{y1} \quad \theta_{z1} \quad u_2 \quad v_2 \quad w_2 \quad \theta_{x2} \quad \theta_{y2} \quad \theta_{z2} \,\} \tag{18}$$

being 1 and 2 the two nodes of the beam, x the axis of the beam, s the subscript defining "section variables", u, v, w the displacements and θ_x, θ_y, θ_z the rotations according to the x, y, z axis respectively (Fig. 4). $[N]$ is the matrix containing the interpolation functions

$$[N] = \begin{bmatrix} N_1 & 0 & 0 & 0 & 0 & 0 & N_2 & 0 & 0 & 0 & 0 & 0 \\ 0 & N_3 & 0 & 0 & 0 & N_4 & 0 & N_5 & 0 & 0 & 0 & N_6 \\ 0 & 0 & N_3^* & 0 & -N_4^* & 0 & 0 & 0 & N_5^* & 0 & -N_6^* & 0 \\ 0 & 0 & 0 & N_1 & 0 & 0 & 0 & 0 & 0 & N_2 & 0 & 0 \\ 0 & 0 & -N_7^* & 0 & N_8^* & 0 & 0 & 0 & -N_9^* & 0 & N_{10}^* & 0 \\ 0 & N_7 & 0 & 0 & 0 & N_8 & 0 & N_9 & 0 & 0 & 0 & N_{10} \end{bmatrix}, \tag{19}$$

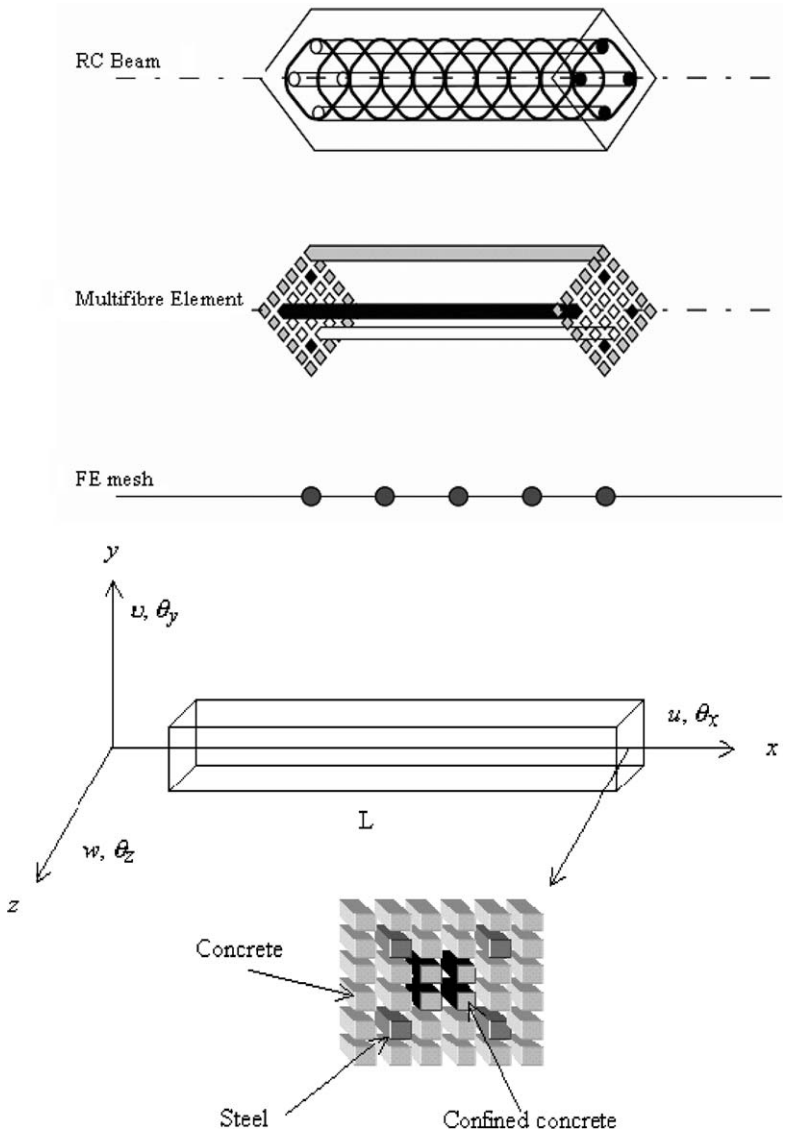

Fig. 4. Using a multifiber beam to model a R/C structural element.

$$N_1 = 1 - \frac{x}{L}; \quad N_2 = \frac{x}{L}; \quad N_3 = \frac{1}{1+\phi}\left\{2\left(\frac{x}{L}\right)^3 - 3\left(\frac{x}{L}\right)^2 - \phi\left(\frac{x}{L}\right) + 1 + \phi\right\}, \tag{20}$$

$$N_4 = \frac{L}{1+\phi}\left\{\left(\frac{x}{L}\right)^3 - \left(2 + \frac{\phi}{2}\right)\left(\frac{x}{L}\right)^2 + \left(1 + \frac{\phi}{2}\right)\left(\frac{x}{L}\right)\right\}, \tag{21}$$

$$N_5 = -\frac{1}{1+\phi}\left\{2\left(\frac{x}{L}\right)^3 - 3\left(\frac{x}{L}\right)^2 - \phi\left(\frac{x}{L}\right)\right\}, \tag{22}$$

$$N_6 = \frac{L}{1+\phi}\left\{\left(\frac{x}{L}\right)^3 - \left(1 - \frac{\phi}{2}\right)\left(\frac{x}{L}\right)^2 - \frac{\phi}{2}\left(\frac{x}{L}\right)\right\}; \quad N_7 = \frac{6}{(1+\phi)L}\left\{\left(\frac{x}{L}\right)^2 - \left(\frac{x}{L}\right)\right\}, \tag{23}$$

$$N_8 = \frac{1}{1+\phi}\left\{3\left(\frac{x}{L}\right)^2 - (4+\phi)\left(\frac{x}{L}\right) + (1+\phi)\right\}; \quad N_9 = -\frac{6}{(1+\phi)L}\left\{\left(\frac{x}{L}\right)^2 - \left(\frac{x}{L}\right)\right\}, \tag{24}$$

$$N_{10} = \frac{1}{1+\phi}\left\{3\left(\frac{x}{L}\right)^2 - (2-\phi)\left(\frac{x}{L}\right)\right\}, \tag{25}$$

with $N_i^* = N_i(\phi^*)$, ϕ and ϕ^* the stiffness ratios due to flexion and shear according to

$$\phi = \frac{12}{L^2}\left(\frac{\int_S Ey^2\,\mathrm{d}S}{\int_S G\,\mathrm{d}S}\right) \quad \text{and} \quad \phi^* = \frac{12}{L^2}\left(\frac{\int_S Ez^2\,\mathrm{d}S}{\int_S G\,\mathrm{d}S}\right) \tag{26}$$

L being the length and S the section of the beam, E and G Young's and shear moduli of the fiber.

For slender structures ϕ and ϕ^* equal zero and the resulting stiffness and mass matrices are reduced to the ones of the Euler–Bernoulli beam theory. The interpolations functions depend on the materials properties and are calculated only once, during the first step (a loop at the section level helps defining the properties of the material of each fiber. After that, the interpolations functions are kept constant). If $\{F\}$ and $\{D\}$ are the section "generalized" stresses and strains respectively, the section stiffness matrix $[K_s]$ is calculated as [18]

$$\{F\} = [K_s]\{D\} \quad \text{with } \{F\}^T = \{\, N \quad T_y \quad T_z \quad M_x \quad M_y \quad M_z \,\}, \tag{27}$$

with N and T axial and shear forces respectively and M moments

$$\{D\}^T = \{\, [u_s'(x)] \quad [v_s'(x) - \theta_{sz}(x)] \quad [w_s'(x) + \theta_{sy}(x)] \quad [\theta_{sx}'(x)] \quad [\theta_{sy}'(x)] \quad [\theta_{sz}'(x)] \,\}, \tag{28}$$

$$[K_s] = \begin{bmatrix} K_{s11} & 0 & 0 & 0 & K_{s15} & K_{s16} \\ & K_{s22} & 0 & K_{s24} & 0 & 0 \\ & & K_{s33} & K_{s34} & 0 & 0 \\ & & & K_{s44} & 0 & 0 \\ & & & & K_{s55} & K_{s56} \\ \text{sym} & & & & & K_{s66} \end{bmatrix}, \tag{29}$$

$$K_{s11} = \int_S E\,\mathrm{d}S; \quad K_{s15} = \int_S Ez\,\mathrm{d}S; \quad K_{s16} = -\int_S Ey\,\mathrm{d}S; \quad K_{s22} = k_y\int_S G\,\mathrm{d}S, \tag{30}$$

$$K_{s24} = -k_y\int_S Gz\,\mathrm{d}S; \quad K_{s33} = k_z\int_S G\,\mathrm{d}S; \quad K_{s34} = k_z\int_S Gy\,\mathrm{d}S, \tag{31}$$

$$K_{s44} = \int_S G\left(k_z y^2 + k_y z^2\right)\mathrm{d}S; \quad K_{s55} = \int_S Ez^2\,\mathrm{d}S; \quad K_{s56} = -\int_S Eyz\,\mathrm{d}S, \tag{32}$$

$$K_{s66} = \int_S Ey^2\,\mathrm{d}S. \tag{33}$$

k_y, k_z shear correction factors dependent upon the material definition and cross section geometry [17].

4. Applications

4.1. Bending of a R/C column

The implementation of the element was made in the library FEDEAS [19] of the finite element code FEAP [20]. In order to validate the performance of the proposed numerical strategy the 3D multifiber Timoshenko element is used hereafter to simulate the inelastic behavior of a column under a general three dimensional load history, tested in the Joint Research

Center in Italy [21]. The specimen has a 0.25-m-square cross section, a free length of 1.5 m and is considered fixed at the base. Longitudinal reinforcement consisted of eight 16 mm diameter bars, uniformly distributed around the perimeter of the section. The concrete cover of the stirrups is 15 mm thick (Fig. 5). Reinforcement bars showed yield stress and ultimate strength of 460 MPa and 710 MPa respectively, the latter at a uniform elongation of 11%. Two tests are simulated (the tests S1 and S7 of the experimental campaign [21]): For the first test uniaxial displacement cycles in pairs of linearly increasing amplitude are alternately applied in the two transverse directions at the top of the column—Figs. 5 and 6(a). During the second test the column is bi-axially displaced according to the nested squares centered at the origin presented in Figs. 5 and 6(b)—four displacement squares are applied with half-side lengths of 0.04 m, 0.06 m, 0.08 m and 0.10 m. A constant axial force of 0.21 MN is applied during both tests, through the center of a loading plate at the top of the column with an actuator located inside a steel-cup-shaped chamber. The chamber is secured in place through two vertical steel arms, which pass through the column base and exert the resultant reaction force at the center of the bottom face of the foundation block. In this way second-order ($P - \Delta$) effects are avoided.

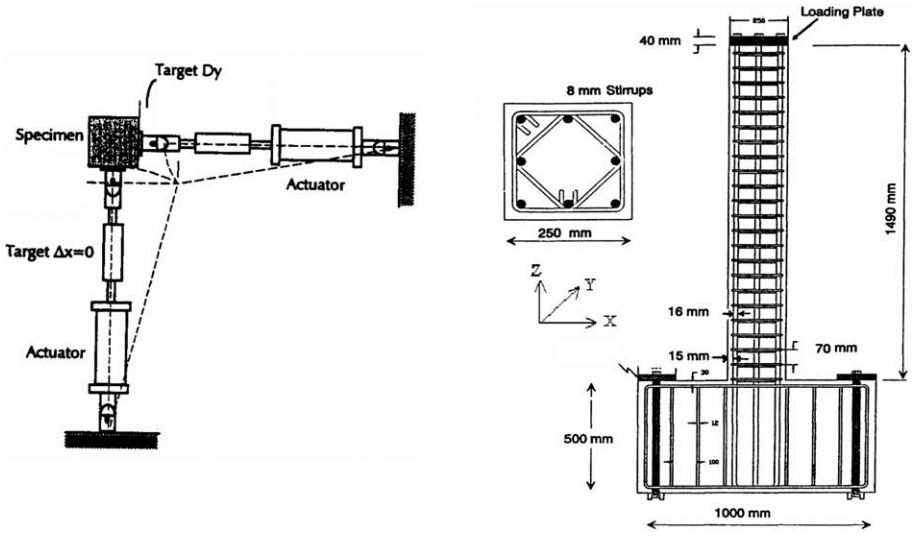

Fig. 5. R/C column: description of the specimen and the experimental setup [21].

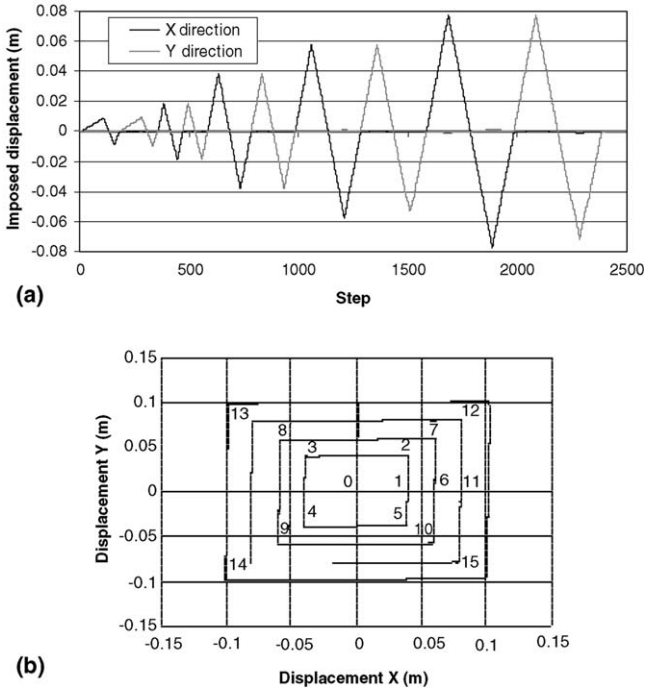

Fig. 6. R/C column: displacement load histories: (a) first test and (b) second test.

Ten multifiber Timoshenko beam elements having 2 Gauss points are used to model the column. Each section has 36 fibers for concrete and 8 fibers for steel. Base slab is not simulated and the specimen is considered fixed at the base. 1D constitutive laws are adopted for concrete and steel based on damage mechanics and plasticity respectively (shear and torsion are considered linear) [10]. Confinement effects are not considered. In order to resolve the non-linear equations the iterative implicit Newton–Raphson solution procedure is followed, where the secant stiffness matrix is used insuring convergence in most cases. This choice leads to a linear rate of convergence instead of the quadratic rate of the classical Newton–Raphson scheme [22], but is usually the choice when using constitutive laws based on damage mechanics [23]. Specific values for the materials are presented in Tables 1 and 2. Comparison of the numerical and experimental results for the eight levels of loading is represented in Figs. 7 and 8. The model simulates correctly the global behavior of the mock-up in terms of displacements and forces in both directions. Calculation is not time consuming (less than one hour with a modern computer) and allows for parametrical studies.

In order to evaluate the effectiveness of the proposed beam element, a second analysis of the S7 test using a coarser mesh is presented in Fig. 9. The number of fibers in the section is again equal to 36. Results are quite similar to the ones using a dense mesh and the hysteretic cycles are well reproduced.

4.2. U-shaped wall submitted to cyclic loading

The second example concerns the experimental results of a R/C U-shaped wall tested at the reaction wall of the ELSA laboratory at JRC Ispra [24]. The 3.6 m height—1.0 scaled—specimen is composed of the U-shaped wall, a lower slab and an upper slab and its design follows Eurocode 8 provisions (Fig. 10). The upper slab is used as the horizontal load application point while six vertical post-tensioning bars apply a normal force of 2 MN. These bars are disposed in such a way that the force is applied close to the inertial center in order to avoid spurious bending on the structure. Torsional rotation is prohibited during the tests inducing important shear stresses in the specimen. The wall is loaded in both directions according to "the butterfly path" presented in Fig. 10.

Eleven multifiber Timoshenko beam elements are used for the numerical simulation of the U-shaped wall. 177 fibers simulate the concrete and 46 fibers the steel. Two Gauss points are considered at each element. Base slab is not simulated and the wall is considered fixed at the base. The behavior of the top slab is considered linear elastic and rotation of the upper part is prohibited in order to reproduce correctly the boundary conditions of the test. The uniaxial version of the La Borderie damage constitutive law is used for concrete (shear and torsion are considered linear). In order to take into account the influence of the stirrups the compression strength of the confined concrete is increased up to 30 MPa. The properties of the materials used for the calculations are presented in Tables 3 and 4.

Comparison of numerical and experimental results for the eight steps of loading is represented in Fig. 11 (A, B, C letters refer to Fig. 10). Again the secant Newton–Raphson scheme is used and the calculation takes only a couple of hours. One

Table 1
R/C column: material parameters for concrete

La Borderie damage model	
Young's modulus	20000 MPa
Poisson coefficient	0.2
A_1	6000 MPa^{-1}
A_2	5 MPa^{-1}
B_1	1
B_2	1.6
β_1	1 MPa
β_2	−40 MPa
Y_{01}	3.8×10^{-4} MPa
Y_{02}	9×10^{-2} MPa
σ_f	3.5 MPa

Table 2
R/C column: material parameters for steel

Steel	
Young's modulus (steel)	200000 MPa
Yield strength	460 MPa
Ultimate strength	710 MPa
Ultimate deformation	11%

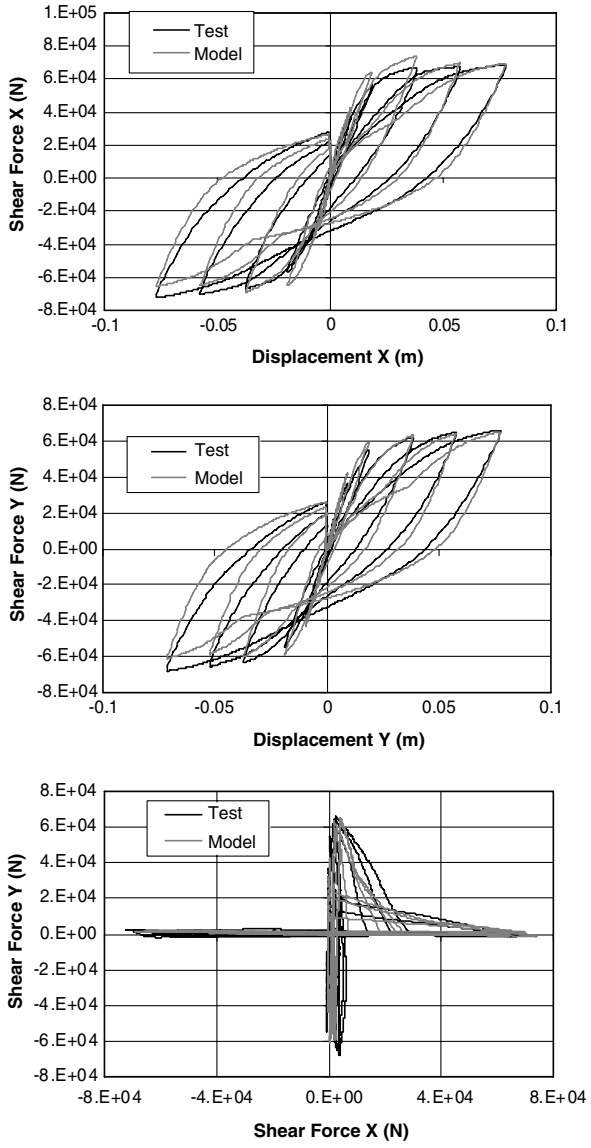

Fig. 7. R/C Column (first test): numerical vs experimental results.

can observe the ability of the model to simulate the global behavior of the specimen in terms of displacements and forces in both directions up to failure. However, differences on the hysteretic loops of the numerical and experimental model are more apparent than in the first two examples. This difference is attributed probably to the effect of non-linear shear stresses that are not taken into account. The specimen is mainly responding in shear to resist high torsion.

5. Multifiber beam accounting for torsion

The analysis of concrete structures subject to severe loading including torsion can be apprehended in different ways depending on the level of refinement and accuracy needed. Following the recent developments in structural mechanics, complete non-linear 3D computations are now feasible. Although the question of material modeling is accurately treated even for complex loading paths (see [25] for a recent development), some assumptions and simplifications should be made when large-scale computations are needed.

One possibility is to stay within the classical beam theory and to use a global formulation taking into account the normal, flexural and torsional interactions [26,27]. This approach allows handling large-scale structures with low computational cost but has the disadvantage of loosing important information on the local level. Classical 3D finite element computations may also be used in linear elasticity in order to treat the problem of general warping of an homogeneous elastic beam [28] or of a composite material like a R/C bar [29]. Modeling of the non-linear behavior of the cross section of a concrete beam can also be done using the Finite Volume Method [30].

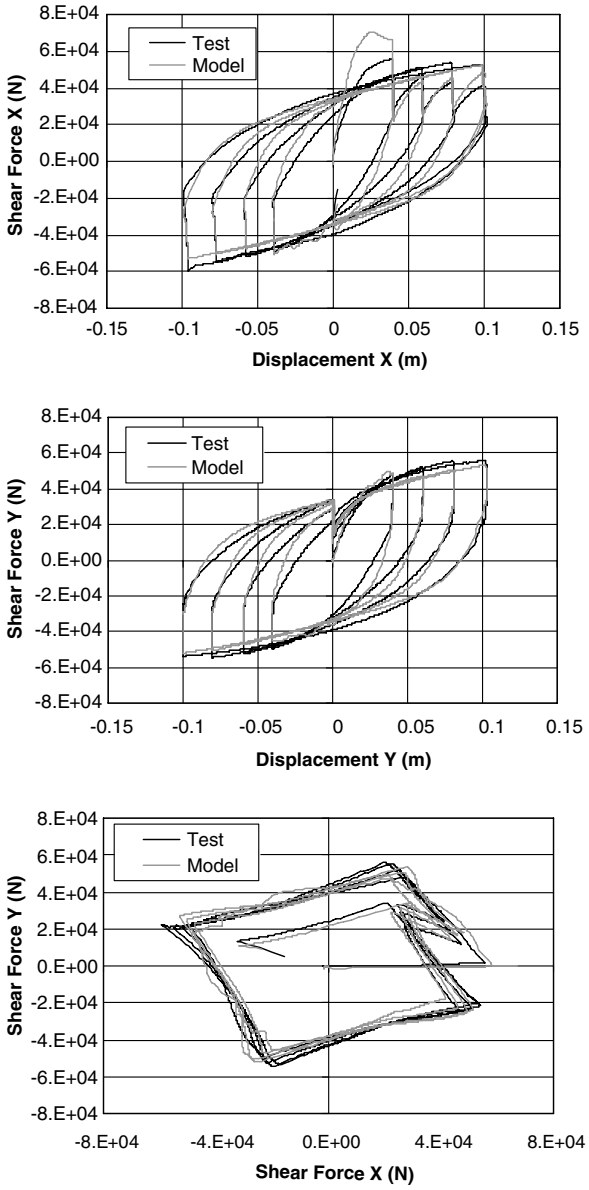

Fig. 8. R/C Column (second test): numerical vs experimental results.

In order to simulate correctly torsional behavior using multifiber beams, the influence in the crack pattern of the section has to be considered. There are various ways:

- *linear*: generally used,
- *globally non-linear*: with a non-linear relation connecting torque moment and rotation,
- *locally non-linear*: by using a 3D local behavior on each fiber. This approach is difficult because very few concrete constitutive relations are efficient and robust enough under cyclic or dynamic loading. Moreover, two possibilities appear: with or without section warping. The relevancy of considering complex kinematics of the section and 3D local constitutive relationships in the framework of a simplified approach is discussed in the following.

5.1. Linear elastic torsion and warping

The aim of the study is to obtain the strain field due to pure torsion for each fiber by solving the warping problem for a section composed of several materials (for example reinforced concrete). Initially the problem is solved within the linear elastic framework of the free torsion of Saint Venant.

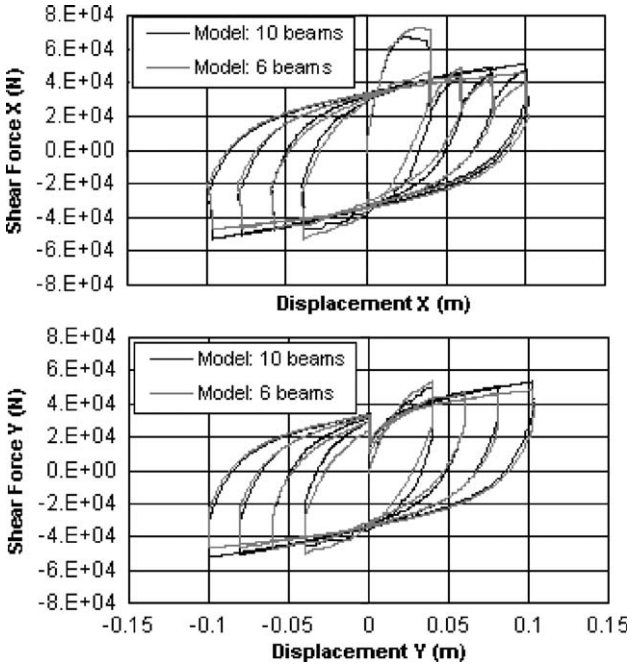

Fig. 9. R/C Column (second test): results of the numerical model using different number of Timoshenko multifiber beam elements.

Let us consider a R/C section assuming that there is no discontinuity between steel and concrete. Under the hypothesis of small displacements, the solution of the problem is assumed as

$$u(x,y,z) = \alpha \cdot \varphi(y,z), \quad v(x,y,z) = -\alpha \cdot x \cdot z \quad \text{and} \quad w(x,y,z) = \alpha \cdot x \cdot y, \tag{34}$$

where u, v, w are the three components of the displacement vectors, (O,x,y,z) is the Cartesian frame reference (Fig. 12), $\varphi(y,z)$ the warping function of the section, $\alpha = (\theta_2 - \theta_1)/L$, $\vec{x}$ is the longitudinal axis of the beam (length L) and θ_1 and θ_2 denote the rotation of its two edges. Solution of the problem consists in defining the displacement field $\vec{U}(u,v,w)$ under an external load $\vec{M}x$ that respects the equilibrium equations, the boundary conditions and the constitutive equations (linear elasticity). The classical solution follows as

$$\Delta\varphi(y,z) = 0. \tag{35}$$

5.2. Numerical implementation [31]

In order to solve this plane problem for a section composed of several materials, a warping-conduction analogy method is used [32]. The problem of the calculation of the warping function for a section made up of several elastic materials (shear modulus G_i) is transformed into a problem of 2D conduction in a plate made up of several materials (thermal conductivity λ_i). Indeed, the solution of Laplacian equations is trivial in heat transfer. Thus, if the boundary conditions are known, the problem can be solved with a usual finite element code.

The notations for the mechanical problem of torsion warping are: $\varphi(y,z)$ is the warping function—homogeneous with a displacement squared—and G_i the shear modulus of the elastic material i.

For the thermal conduction problem, notations are as follows: $T(y,z)$ is the temperature function, λ_i is the thermal conductivity of the isotropic material i and $\Phi(y,z) = \lambda \operatorname{grad} T(y,z)$ the thermal density flux.

For torsion one obtains $\Delta\varphi(y,z) = 0$ in the surface of each material. This equation corresponds to the equation of heat for conduction in steady state $\Delta T(y,z) = 0$. The shear modulus of the elastic material G_i is equivalent to λ_i, the thermal conductivity of the isotropic material.

In order to find the boundary conditions on external contour for torsion, one writes that there are no external forces applied to the contour of the section (external surface of the beam), with n, the unit vector leaving normal to contour $\mathrm{d}S$, of component n_y and n_z. Continuity between two materials is expressed by insuring continuity of the function $\varphi(y,z)$ and continuity of the forces on the border between two materials.

The conduction problem equivalent to the torsion warping function problem is as follows:

$$\Delta T(y,z) = 0. \tag{36}$$

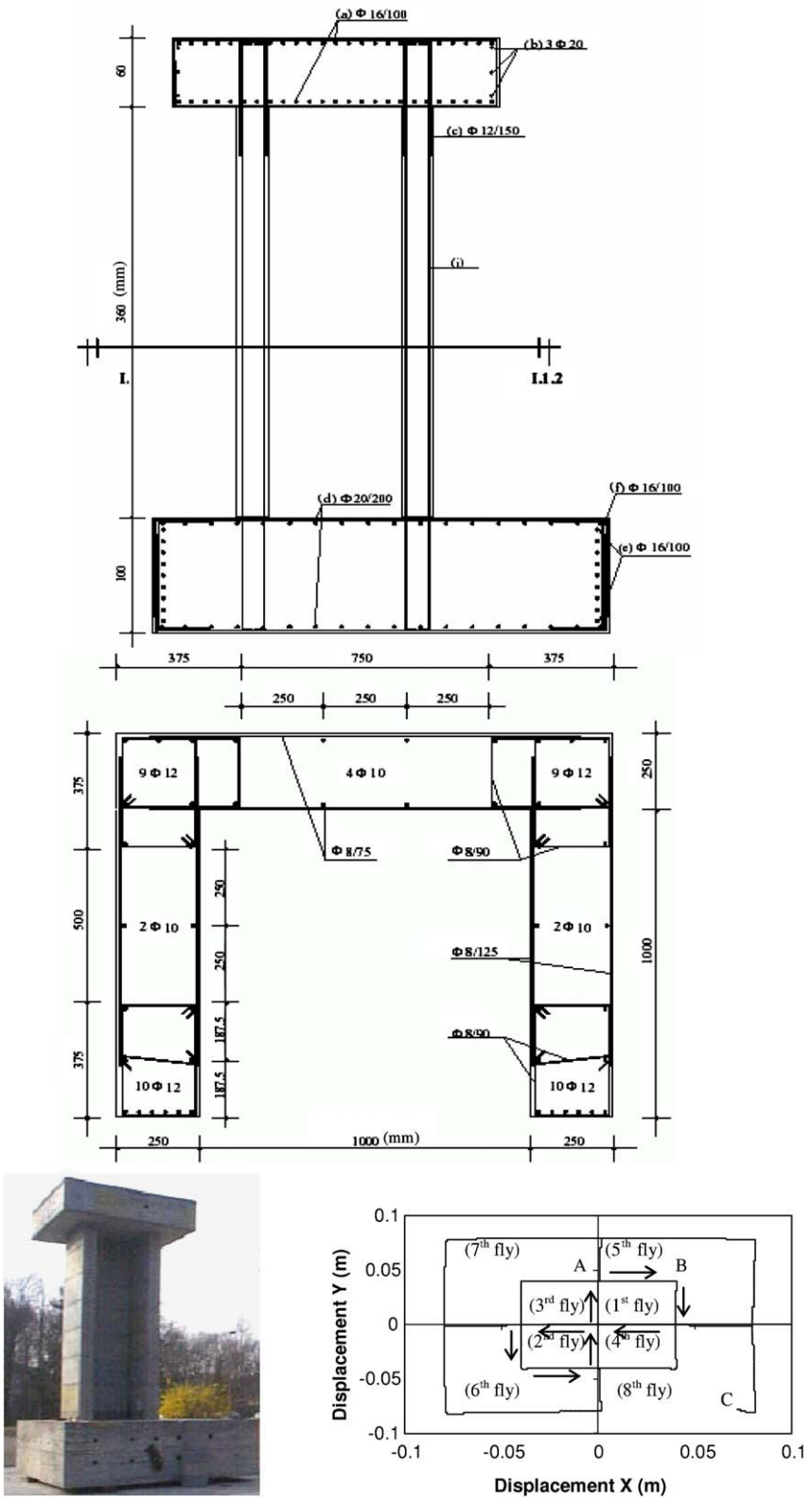

Fig. 10. U-shaped wall: description of the specimen and loading history.

For the flow imposed on the free face:

$$\underline{\Phi}_i \cdot \underline{n} = \begin{bmatrix} \lambda_i z \\ -\lambda_i y \end{bmatrix} \begin{bmatrix} n_y \\ n_z \end{bmatrix} \tag{37}$$

Table 3
U-shaped wall: material parameters for concrete

La Borderie damage model	
Young's modulus	28 900 MPa
Poisson coefficient	0.25
A_1	6000 MPa^{-1}
A_2	5 MPa^{-1}
A_2 (confined)	6.7 MPa^{-1}
B_1	1
B_2	1.6
β_1	0.4 MPa
β_1 (confined)	1 MPa
β_2	−40 MPa
Y_{01}	2.3×10^{-4} MPa
Y_{02}	0.1×10^{-2} MPa
σ_f	3.5 MPa

Table 4
U-shaped wall: material parameters for steel

Steel	
Young's modulus (steel)	200 000 MPa
Yield strength	515 MPa
Ultimate strength	615 MPa
Ultimate deformation	24%

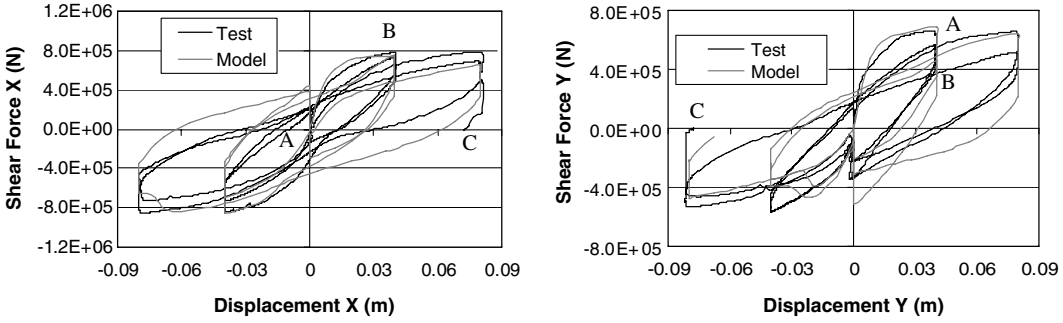

Fig. 11. U-shaped wall: numerical vs experimental results.

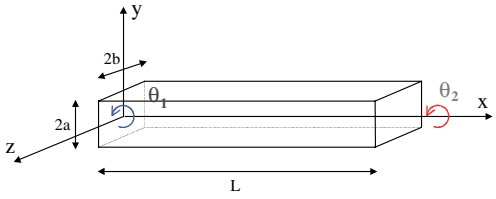

Fig. 12. Beam model in torsion.

and "jump" of flow imposed between two materials:

$$(\underline{\Phi}_i - \underline{\Phi}_j) \cdot \underline{n}_i = \begin{bmatrix} (\lambda_i - \lambda_j)z \\ (-\lambda_i + \lambda_j)y \end{bmatrix} \begin{bmatrix} n_y^i \\ n_z^i \end{bmatrix}. \tag{38}$$

Thus, by applying these boundary conditions, the problem can be solved with any finite element code able to solve thermal conduction problems (the following computations are made using the finite element code CASTEM 2000).

This warping function calculation method is used to determine the torsion shear strains all over a beam section:

$$\boldsymbol{\varepsilon} = \begin{bmatrix} 0 & \frac{1}{2}\alpha\left(\frac{\partial\varphi}{\partial y} - z\right) & \frac{1}{2}\alpha\left(\frac{\partial\varphi}{\partial z} + y\right) \\ \frac{1}{2}\alpha\left(\frac{\partial\varphi}{\partial y} - z\right) & 0 & 0 \\ \frac{1}{2}\alpha\left(\frac{\partial\varphi}{\partial z} + y\right) & 0 & 0 \end{bmatrix}. \tag{39}$$

As in [28], the torque moment is obtained by integrating the stresses at the elastic torsion center:

$$Mx = \int_S (y\sigma_{xz} - z\sigma_{xy})\,\mathrm{d}S. \tag{40}$$

The multifiber framework is a natural integration domain allowing an easy numerical implementation of this approach into any general-purpose finite element code.

5.3. Non-linear extension

The crack pattern initiated by torsion is assumed to remain constant during crack propagation after nucleation. The strain field along the cross section due to torsion and warping may initiate the non-linear behavior but the global shape of the crack pattern is not be affected by local damage. The warping function is thus computed on the basis of a linear elastic material and is kept constant during the non-linear range.

6. Application

6.1. Torsion of plain concrete beams

The experimental studies used hereafter are from [33]. Several plain concrete beams have been tested in pure torsion. The beams are composed of three parts: two reinforced end parts (properly reinforced, so as to remain elastic) and one plain concrete part in the middle (where cracking and failure occurred during the tests). A pure torsion loading is applied at both ends of the beams (Fig. 13). The beams are supported on two roller supports 1.30 apart, ensuring that the beam is free to twist and to elongate longitudinally. Two types of sections are investigated: a rectangular section specimen (R test) and a T-section specimen (T test) (Fig. 14).

Calculations of the warping functions are carried out for the two specimens. Non-linear calculations of the concrete sections in pure torsion are also presented. It is thus possible to compute the stresses using the local scalar damage constitutive relation [9]. The parameters used for the materials are fixed from the experimental compression and tension tests results of the R test. However, as the Young's modulus was unknown it is taken equal to 25 000 MPa allowing reproducing the experimental initial stiffness and ν, the Poisson ratio, equal to 0.2. The material parameters used for the computation are given in Table 5.

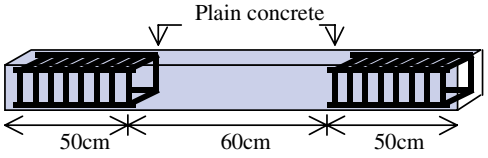

Fig. 13. Plain concrete beam under pure torsion.

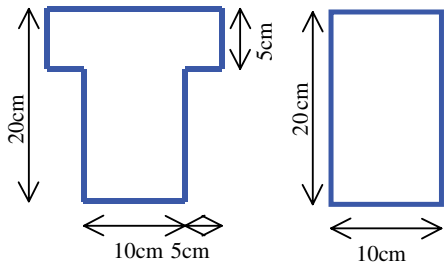

Fig. 14. T and rectangular cross sections.

Table 5
Plain concrete beam: material parameters for concrete

Mazars damage model	
Young's modulus	25 000 MPa
Poisson coefficient	0.2
Initial threshold ε_{d0}	1×10^{-04}
$A_{\text{Compression}}$	1.4
$B_{\text{Compression}}$	1900
A_{tension}	0.8
B_{tension}	17 000
Shear correction β	1.06

The calculated warping functions for both sections are presented in Fig. 15. In order to highlight the importance of the warping function for the initial stiffness but also in the non-linear range, two types of analysis have been carried out: either by taking into account the warping function, or by neglecting it (i.e. by giving it a zero value all over the sections). For both sections, the curves giving the evolution of the torque moments (by integrating the stresses upon the section) with the rotation angle are plotted in Figs. 16 and 17. Those results show the importance of considering the warping function in order to reproduce correctly the experimental results. The model without the warping function has an initial elastic stiffness higher than the model considering warping. The maximum torque moment is also poorly evaluated. This can be explained by the fact that the warping function modifies a lot the strain distribution in the section before crack initiation, and thus the damage in the section, as shown in Fig. 18. Even though the estimation of the cross section shear strain field using warping is necessary to describe correctly the maximum bearing capacity of a reinforced concrete member under torsional loading, the basic assumption made in computing this warping function (constant) seems to be adequate.

The damage patterns in Fig. 18 show that the pattern without warping is similar to the one of a circular section (where no warping occurs—damage is almost zero near the center of the section) and completely different from the one considering warping. This has a crucial consequence on the bending behavior of a beam subjected to both torsion and bending. In Fig. 19, the evolution of its bending stiffness is studied, while applying a pure torsion loading and using two types of model: with and without warping. At crack initiation, both models give the same response in terms of stiffness. While cracks propagate in the cross section, the two different damage profiles induce a completely different behavior for bending.

Work is in progress in order to apply the proposed modeling strategy to a R/C section.

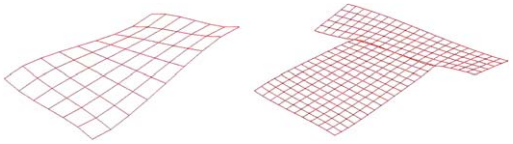

Fig. 15. Warping function obtained for the rectangular and T-cross sections.

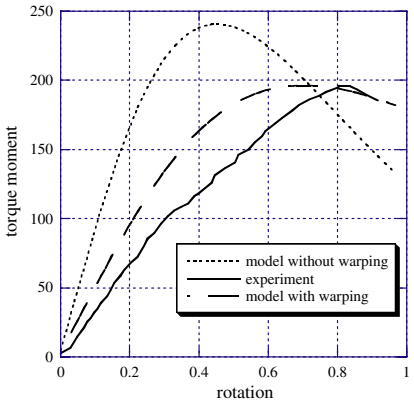

Fig. 16. R test: torque moment (kN cm) vs rotation (10^{-4} rad/cm) comparisons.

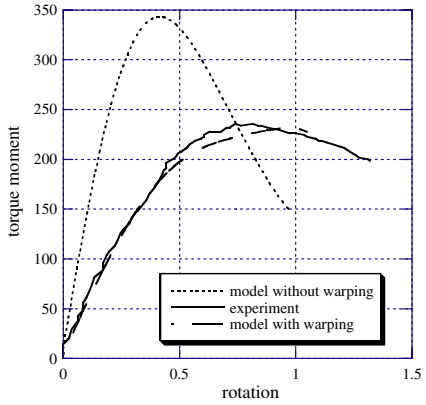

Fig. 17. T test: torque moment (kN cm) vs rotation (10^{-4} rad/cm) comparisons.

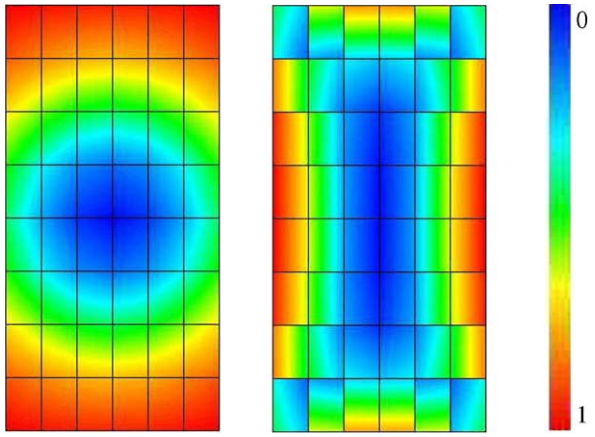

Fig. 18. R test: damage field on the rectangular cross section, without and with warping.

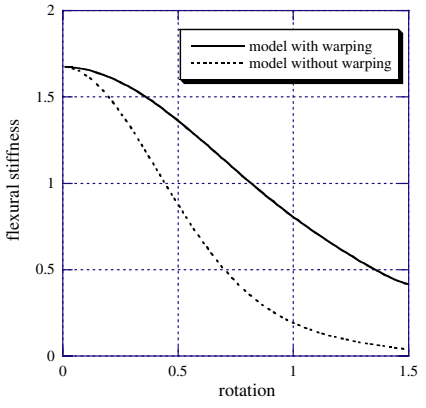

Fig. 19. Flexural stiffness evolution (10^6 N m) in function vs rotation (10^{-4} rad/cm) for a model with or without warping.

7. Conclusions

This work investigates the use of multifiber beam elements in order to account for shear and torsion. Constitutive laws are based on damage mechanics and plasticity and applications are presented for concrete structural elements. More specifically:

At the first part of the paper, the formulation of a Timoshenko multifiber beam element is elaborated. The element has higher order interpolations functions to avoid any shear locking phenomena. The element is used successfully to simulate the global response of R/C columns and U-shaped walls subjected to complex biaxial loading.

For those simulations, shear stresses are considered linear and torsion and shear are uncoupled. However, the formulation of the Timoshenko element is presented in a general way and so the element is ready to be used, without any further development, with models able to couple shear and torsion. The implementation of a 3D robust constitutive model for concrete under cyclic loading would certainly improve the results at the global but also at the local level.

It is necessary though to mention the fact that the behavior of R/C sections under shear (or torsion) is a result of the anisotropic response of the R/C section with cracks developed at a certain inclination with respect to the section's plane. The use of isotropic damage models and Timoshenko kinematics (where shear stresses are considered constant in the section) limits the domain of application of the proposed strategy to a slenderness more or less close to 1. This is for example shown for the case of R/C concrete walls having very small slenderness (equal to 0.4) in [34]. A solution—always within the family of simplified models—is to use some type of truss-analogy models that transfer forces to the longitudinal and transverse reinforcements (Strut-and-Tie models [35], the Compression Field Theory [36], the Rotating-Angle-Softened Truss model [37], the Equivalent Reinforced Concrete [12,34,38]). The reader can find a detailed presentation of some truss-analogy models in [39].

Furthermore, it is now well known that the use of local constitutive relationships provides results that are mesh-dependent in the post-cracking regime. Localized failure is caused by strain softening, which cannot be described by classical models, because they lack a length scale. The use of a non-local damage model [40] or a local strain-gradient model [41,42] can provide a remedy in this particular problem.

At the second part of the paper it is shown that for a non-linear analysis with multifiber beams subject to torsion, the introduction of warping is crucial in order to reproduce the torque—rotation evolution. Damage profiles are completely different depending on considering or not warping and consequently the global behavior is modified: torsion and bending stiffness, maximum torque, etc. In this paper the assumption made is that the warping function is constant, determined on elastic assumptions even during crack propagation. The model gives good results for rectangular sections as well as for T-sections in accordance with the experimental results. The next step will be to test the proposed strategy for R/C sections under cyclic loading.

Acknowledgements

The authors would like to thank Pr. Boussias S. from the University of Patras and Pr. Karayannis C.G. from the Democritus University of Thrace (Greece) for providing the experimental results. Part of this work was granted from the European program ICONS [43].

References

[1] T. Paulay, Capacity design of reinforced concrete ductile frames, in: Proceedings, Workshop on Earthquake-Resistant Reinforced Concrete Building Construction, University of California at Berkeley, III, 1970, pp. 1043–1075.
[2] T. Paulay, M.J.N. Priestley, Seismic Design of Reinforced Concrete and Masonry Buildings, Wiley, John & Sons, Incorporated, 1992.
[3] M.J.N. Priestley, Myths and Fallacies in Earthquake Engineering, Revisited. The Mallet Milne Lecture, IUSS Press, 2003.
[4] A.K. Chopra, Dynamics of Structures: Theory and Applications to Earthquake Engineering, second ed., Prentice-Hall, 2001.
[5] A.S. Elnashai, Advanced inelastic static (pushover) analysis for earthquake applications, J. Struct. Engrg. Mech. 12 (1) (2001) 51–69.
[6] P. Fajfar, A nonlinear analysis method for performance-based seismic design, Earthquake Spectra 16 (3) (2000) 573–592.
[7] J. Lemaitre, J.L. Chaboche, Mechanics of Solids Material, Cambridge University Press, 1990.
[8] P.J. Armstrong, C.O. Frederick, A Mathematical Representation of the Multiaxial Bauschinger Effect, G.E.G.B. Report RD/B/N 731, 1966.
[9] J. Mazars, A description of micro- and macroscale damage of concrete structures, J. Engrg. Fracture Mech. 25 (5/6) (1986) 729–737.
[10] Ch. La Borderie, Phénomènes unilatéraux dans un matériau endommageable: modélisation et application à l'analyse de structures en béton, Ph.D. thesis, Univ. Paris VI, 1991.
[11] P. Kotronis, Cisaillement dynamique de murs en béton armé, Modèles simplifiés 2D et 3D. Ph.D., LMT—Ecole Normale Supérieure de Cachan, 2000.
[12] P. Kotronis, J. Mazars, Simplified modelling strategies to simulate the dynamic behaviour of R/C walls, J. Earthquake Engrg. 9 (2) (2005) 285–306.
[13] P. Kotronis, L. Davenne, J. Mazars, Poutre 3D multifibre Timoshenko pour la modélisation des structures en béton armé soumises à des chargements sévères, Rev. Française Génie Civil 8 (2–3) (2004) 329–343.
[14] M. Petrangeli, P.E. Pinto, V. Ciampi, Fiber element for cyclic bending and shear of RC structures. I: Theory, J. Engrg. Mech. 125 (9) (1999) 994–1001.
[15] E. Spacone, F.C. Filippou, F.F. Taucer, Fiber beam-column model for nonlinear analysis of R/C frames. I: Formulation, Earthquake Engrg. Struct. Dynam. 25 (7) (1996) 711–725.
[16] Z. Friedman, J.B. Kosmatka, An improved two-node Timoshenko beam finite element, Comput. Struct. 47 (3) (1993) 473–481.
[17] G.R. Cowper, The shear coefficient in Timoshenko's beam theory, ASME J. Appl. Mech. 33 (1966) 335–340.
[18] J. Guedes, P. Pégon, A. Pinto, A fibre Timoshenko beam element in CASTEM 2000, Special publication Nr. I.94.31, J.R.C., I-21020, Ispra, Italy, 1994.
[19] F.C. Filippou, Nonlinear static and dynamic analysis for evaluation of structures, in: 3rd European Conference on Structural Dynamics Eurodyn 96, Florence, Italy, 1996, pp. 395–402.
[20] R.L. Taylor, FEAP: A finite element analysis program, version 7.3 manual, University of California, Berkeley, 2000.

[21] S.N. Bousias, G. Verzeletti, M.N. Fardis, E. Guiterrez, Load-path effects in column biaxial bending and axial force, J. Eng. Mech. ASCE 121 (5) (1995) 596–605.
[22] M.A. CrisfieldNonlinear Finite Element Analysis of Solids and Structures, vol. I, John Wiley, Chichester, 1991.
[23] J. Mazars, G. Pijaudier-Cabot, Continuum damage theory—application to concrete, ASCE J. Engrg. Mech. 115 (1989) 345–365.
[24] P. Pégon, C. Plumier, A. Pinto, J. Molina, P. Gonzalez, P. Tognoli, O. Hubert, U-shaped-wall: description of the experimental set-up, Report, Joint Research Center (J.R.C.), Ispra, Italy, 2000.
[25] V. Kafka, Concrete under complex loading: mesomechanical model of deformation and of cumulative damage, Eur. J. Mech. A/Solids 23 (2004) 63–75.
[26] G.H. Powell, P.F. Chen, 3-D beam-column element with generalized plastic hinges, J. Engrg. Mech. Div. ASCE 112 (7) (1986) 627–641.
[27] W.A. Thanoon, D.K. Paul, M.S. Jaafar, D.N. Trikha, Influence of torsion on the inelastic response of tree-dimensional r.c. frames, Finite Element Anal. Des. 40 (2004) 611–628.
[28] M. Schulz, F.C. Filippou, Generalized warping torsion formulation, J. Engrg. Mech. (1998) 339–347.
[29] Z. Li, J.M. Ko, Y.Q. Ni, Torsional rigidity of reinforced concrete bars with arbitrary sectional shape, Finite Element Anal. Des. 35 (2000) 349–361.
[30] C.G. Karayanis, Torsional analysis of flanged concrete elements with tension softening, Comput. Struct. 54 (1) (1995) 97–110.
[31] G. Casaux, Modélisation tridimensionnelle du comportement sismique d'ouvrages en béton armé—Développement de méthodes simplifiées, Ph.D. thesis LMT- Ecole Normale Supérieure de Cachan, 2003.
[32] J.M. Proix, N. Laurent, P. Hemon, G. Bertrand, Code Aster, manuel de référence, Fascicule R3.08: Eléments mécaniques à fibre moyenne, Document: R3.08.03, Calcul des caractéristiques d'une poutre de section transversale quelconque, 2000.
[33] C.G. Karayannis, C.E. Chalioris, Experimental validation of smeared analysis for plain concrete in torsion, J. Struct. Engrg. 126 (6) (2000) 646–653.
[34] J. Mazars, P. Kotronis, L. Davenne, A new modelling strategy for the behaviour of shear walls under dynamic loading, Earthquake Engrg. Struct. Dynam. 31 (4) (2002) 937–954.
[35] J. Schlaich, I. Schäfer, M. Jennewein, Towards a consistent design of structural concrete, J. Prestress. Concr. Inst. 32 (3) (1987) 74–150.
[36] M.P. Collins, D. Mitchell, Shear and torsion design of prestressed and non-prestressed concrete beams, J. Prestress. Concr. Inst. 25 (5) (1980) 32–100.
[37] T.T.C. Hsu, Toward a unified nomenclature for reinforced concrete theory, J. Struct. Engrg. ASCE 122 (3) (1996) 275–283.
[38] P. Kotronis, J. Mazars, L. Davenne, The equivalent reinforced concrete model for simulating the behaviour of shear walls under dynamic loading, Engrg. Fracture Mech. 70 (7–8) (2003) 1085–1097.
[39] ASCE-ACI Committee 445 on Shear and Torsion, Recent approaches to shear design of structural concrete, J. Struct. Engrg. 124 (12) (1998) 1375–1417.
[40] G. Pijaudier-Cabot, Z.P. Bažant, Nonlocal damage theory, J. Engrg. Mech. 113 (1987) 1512–1533.
[41] R. Chambon, D. Caillerie, T. Matsushima, Plastic continuum with microstructure, local second gradient theories for geomaterials: localization studies, Int. J. Solids Struct. 38 (2001) 8503–8527.
[42] P. Kotronis, R. Chambon, J. Mazars, F. Collin, Local second gradient models and damage mechanics: application to concrete, in: 11th International Conference on Fracture, Turin, Italy, 20–25 March, Org. ICF, cd paper no 5712, 2005.
[43] J.M. Reynouard, M.N. Fardis (Eds.), R.T. Severn, R. Bairrão (Gen. Eds.), CAFEEL-ECOEST/ICONS, Thematic report N.5, Shear Walls Structures, (LNEC, ISBN 972-49-1891-2) September, 2001.